Thermochimica Acta 488 (2009) 54–59

Contents lists available at ScienceDirect

Thermochimica Acta

journal homepage: www.elsevier.com/locate/tca

Sintering kinetics of submicron sized cobalt powder

Bhaskar Paul[a], Dheeraj Jain[b], A.C. Bidaye[a], I.G. Sharma[a], C.G.S. Pillai[b,*]

[a] Materials Processing Division, Bhabha Atomic Research Centre, Mumbai 400 085, India
[b] Chemistry Division, Bhabha Atomic Research Centre, Mumbai 400 085, India

ARTICLE INFO

Article history:
Received 19 August 2008
Received in revised form 1 January 2009
Accepted 7 January 2009
Available online 23 January 2009

Keywords:
Sintering
Kinetics
Cobalt
Dilatometry
SID

ABSTRACT

The paper details the results of sintering kinetics studies on submicron sized fine cobalt metal powders prepared through oxalate decomposition route using both conventional sintering method as well as stepwise isothermal dilatometry (SID) technique. Powder preparation and processing parameters such as decomposition temperature, compaction pressure and sintering atmosphere, etc. were optimized to achieve highest sintered density with lowest activation energy through conventional sintering. Role of submicron sized powder and surface contamination layers on initial shrinkage was explained towards early shrinkage of cobalt compacts by dilatometric analysis. Measured step isothermal shrinkage data were analyzed by Makipirtti–Meng method. The shrinkage data were found to fit well with the rate equation proposed in this method and its validity was established for the metallic systems also. Kinetic parameters were evaluated and sintering was found to occur through three major mechanisms operative successively, which are grain boundary diffusion, lattice diffusion and plastic/viscous flow with the energy of activation as 135, 234 and 373 kJ/mol, respectively. The results were well supported by microstructural analysis of sintered specimens.

1. Introduction

The major use of cobalt metal continues to be in super alloys followed by its use in hard materials, pigments, magnets, batteries, orthopedic alloys, catalysts and coloring agents, etc. Besides this, extensive usage of its radioisotope ^{60}Co, as a gamma radiation source for a variety of industrial and medical applications, self powered neutron detectors (SPNDs), flux mapping, fuel management, etc. makes it a material of applied interest for the researchers [1,2]. As the industrial applications of cobalt are increasing, its reprocessing/recovery from scrape materials such as spent catalyst, used cutting tools, etc. is gaining importance. An efficient flow sheet for recovering high purity cobalt metal from spent ammonia cracker catalyst has previously been established in authors' lab using hydrometallurgical route [3,4]. In this process, the spent catalyst is converted to cobalt oxalate dihydrate $Co(OOC)_2{\cdot}2H_2O$, which then is thermally decomposed in reducing atmosphere to produce submicron sized pure cobalt powder. During decomposition of oxalate, six foreign atoms leave its lattice for each cobalt atom and therefore produce highly porous metal powder with a large specific surface area and fine crystallite size.

These powders are then sintered into different shapes by powder metallurgy and their sintering is mainly governed by powder properties such as particle size, shape/morphology and distribution, etc. Understanding of the sintering mechanism of these powders is therefore very essential from both applied as well as research point of view. Sintering kinetics of cobalt metal powders has been investigated earlier [5–7]. However, for submicron sized powders, which are inherently superior due to their large surface area and higher reactivity as compared to coarse ones, no such report is available.

To address this, sintering studies on submicron sized cobalt powder were carried out using conventional sintering and stepwise isothermal dialatometry (SID), a relatively new approach that has proven its utility in analyzing the sintering mechanism of ceramic powders [8–11]. Using this approach it is possible to evaluate both, the sintering mechanism and activation energies using a single shrinkage data obtained from dialatometry. Observed results from SID were analyzed by a model given by Makipirtti–Meng [8–11]. It has been found that the model fits well to explain the sintering kinetics of metallic powder systems also.

2. Experimental

2.1. Preparation and characterization of submicron sized cobalt powder

Cobalt oxalate dihydrate $Co(OOC)_2{\cdot}2H_2O$, produced by the method reported earlier [3,4] was used for obtaining cobalt metal powder. Dihydrate nature of the oxalate was confirmed by thermo gravimetric analysis. Decomposition of the oxalate was carried out in a specially designed vertical silica reactor with porous plate

* Corresponding author. Tel.: +91 22 25595355; fax: +91 22 25505151/25519613.
E-mail address: cgspil@barc.gov.in (C.G.S. Pillai).

0040-6031/$ – see front matter © 2009 Elsevier B.V. All rights reserved.
doi:10.1016/j.tca.2009.01.017

for gas flow acting as a base for the charge material. The reactor was placed in a resistive tubular furnace and decomposition was performed in flowing Argon–hydrogen atmosphere (80:20 by volume) with a flow rate of 20 ml/min at different temperatures (723, 773, 823 and 873 K) with a soak period of 30 min in each preparation. The contents were cooled to ambient temperature under the same reducing atmosphere and passivated by flowing CO_2 gas (10 ml/min) over the powder before taking the samples out. Elemental analyses of both oxalate and metal powders were carried out on an atomic absorption spectrometer (GBC Spectra Avanta, Model 908). The metal powders were phase characterized by room temperature powder X-ray diffraction patterns recorded on a powder diffractometer (Philips, Model PW 1820 controlled by PW 1710 microprocessor). Silicon was used as an external standard. Particle size of the as-prepared cobalt powder was measured by a laser particle size analyzer (CILAS 1064) using distilled water as dispersant. Powder morphology and particle size were examined in a scanning electron microscope (JEOL, Model JSM-T330A).

2.2. Sintering studies on cobalt metal powder

For conventional sintering studies, the as-prepared metal powders were pressed into cylindrical pellets (6 mm diameter, 4 mm height) at compaction pressures of 150, 200, 250 and 300 MPa and sintered up to 1573 K in Ar–4% H_2 atmosphere with a flow rate of 20 ml/min. Heating rate of 10 K/min and a soak period of 1 h at the peak temperature was kept for all the samples. Densities of sintered pellets measured geometrically, were examined as a function of compaction pressure and powder processing temperature. The highest density was achieved for powder decomposed at 823 K and compacted with a pressure of 250 MPa. These powder processing parameters were adopted for all dilatometric experiments to study sintering kinetics. Green pellets were also sintered in pure argon atmosphere to see the effect of sintering atmosphere on the sintered density.

All dilatometric measurements were carried out in a vertical-type thermo mechanical analyzer (Setsys Evolution TMA 1600, M/s SETARAM, France) with minimum load (1 g) conditions in reducing atmosphere (Ar–4% H_2, 20 ml/min). Shrinkage profiles were recorded by heating the green compacts at 10 K/min. up to the programmed temperature and soaked at that temperature for 1 h followed by cooling to ambient. A sample already sintered at 1573 K for 1 h was also measured separately up to the same temperature with same heating cycle to evaluate the linear thermal expansion behavior of cobalt. The same was subtracted from the as-measured shrinkage data of green compacts to determine true shrinkage behavior. A special sintering schedule was employed for recording the sintering behavior through stepwise isothermal dilatometry (SID). In this experiment, the shrinkage was continuously measured while heating the green pellet from 298 to 823 K at a heating rate of 10 K/min. and then onwards up to 1223 K with the same rate of heating, with an isothermal hold of 30 min at each 50 K interval (step). Green densities (ρ_o) of the pressed samples were measured geometrically where as that of the sintered samples (ρ_s) were measured both dimensionally as well as by Archimedes principle using water as immersion liquid. Microstructures of samples sintered at different temperatures were studied using scanning electron microscopy.

3. Results and discussion

3.1. Powder morphology

The analysis of as-prepared cobalt oxalate dihydrate ($Co(COO)_2{\cdot}2H_2O$) showed 0.052% Ni, 0.005% Al, 0.016% Fe and 0.005% Cu, as other metal impurities. XRD analysis of as-prepared cobalt powder revealed a mixture of both HCP and FCC structure. No detectable peaks for surface carbonates/oxides were observed in the diffraction pattern, which must be due to amorphous nature [6] of these surface monolayers, formed during passivation of the metal powder. Fig. 1 shows the SEM image of cobalt powder prepared at 823 K, which reveals a fibrous morphology. The micron sized maze/sweet corn-like morphology of the powder is mainly due to the spherolitic growth of small spherical individual crystallites as is evident from the inset of Fig. 1. The observed fibrous morphology is possibly due to the tendency of ferromagnetic cobalt crystallites to align in a particular direction and form long chain-like structures. Also, as the powder is prepared above 673 K, adhesion between individual particles results into agglomeration of the powder. The average agglomerate size measured from SEM images is 23 (±3) μm, close to that evaluated through laser particle size analyzer, i.e. 12, 18 and 23 μm for powders prepared at 773, 823 and 873 K, respectively. It is to be noted that unavailability of suitable dispersant for the particle size analysis resulted in average agglomerate size determination and not the crystallite size. However, the average crystallite size, clearly visible in the inset of Fig. 1 is around 200 nm and reveals the submicron nature of the metal powder.

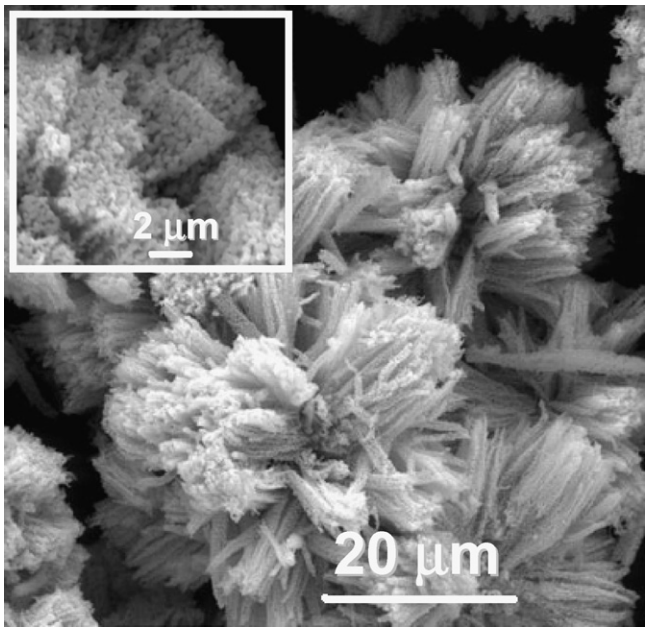

Fig. 1. SEM image of cobalt powder prepared from oxalate decomposition at 823 K. Inset shows the higher magnification image of agglomerated particle to show submicron nature of the powder.

3.2. Sintering by conventional method

Shrinkage analysis of a green compact during its initial stage of sintering is given by the well-known Arrhenius function [7,12],

$$T^{2/p}\left(\frac{\Delta l}{l_o}\right) = K\exp\left(\frac{-2Q}{pRT}\right) = K'\exp\left(\frac{-Q_a}{RT}\right) \quad (1)$$

where

$$K = \frac{B_o t}{(2^p D^q R)^{2/p}} \quad (2)$$

$$Q = \frac{pQ_a}{2} \quad (3)$$

and $T^{2/p}(\Delta l/l_0)$ = shrinkage parameter

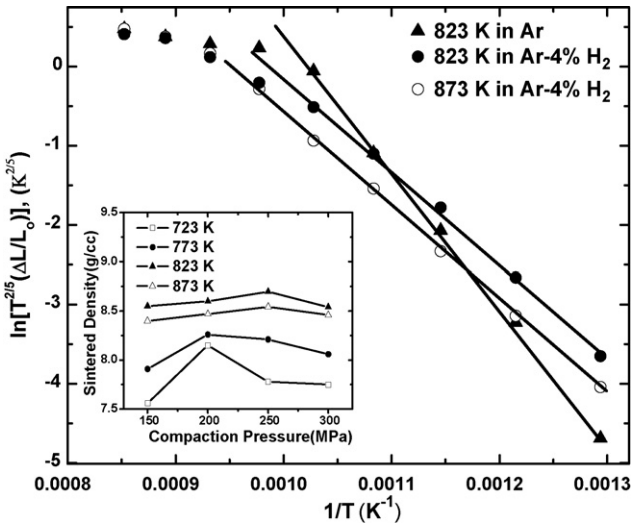

Fig. 2. Arrhenius plots for the shrinkage parameter of cobalt powder compacts sintered up to 1523 K under different preparation temperatures and sintering atmospheres. Inset shows the variation of sintered density as a function of powder preparation temperatures and compaction pressures.

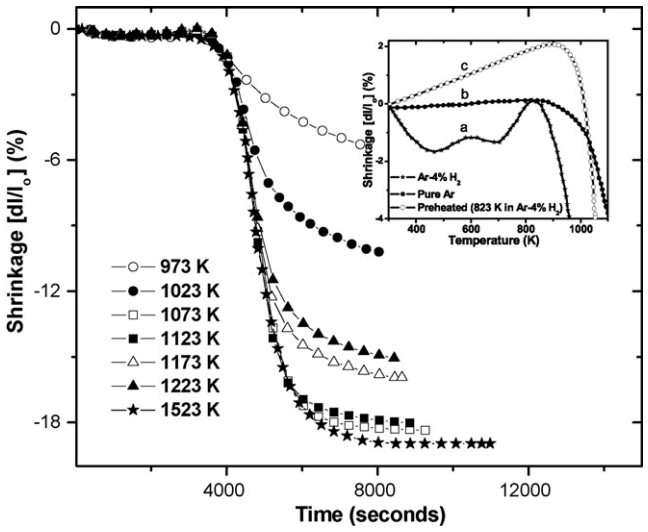

Fig. 3. Dilatometric shrinkage curves recorded on cobalt green compacts up to different sintering temperatures in Ar–4% H_2 atmosphere. Inset shows the early shrinkage due to fine particle size and surface contamination reduction.

Here, Δl is the change in sample length due to shrinkage, l_o, the initial length, B_o, a constant dependent upon material properties, t, the sintering time, D, the particle diameter, R, the gas constant, T, the absolute temperature and K', a constant. Q is the activation energy of mass diffusion and depends upon the sintering mechanism operative whereas Q_a is apparent activation energy that is determined experimentally. Parameters p and q depend upon the sintering mechanism operative at a certain stage and take up different values as $(p, q) = (2, 1), (5, 3), (6, 4)$ and $(7, 4)$ for viscous/plastic flow, lattice/volume diffusion, grain boundary diffusion, and surface diffusion, respectively.

Above methodology was adopted to analyze the conventional sintering data in the present work and the value of $(\Delta l/l_o)$ was taken as $(\rho_s - \rho_o)/\rho_s$ where ρ_s and ρ_o represents the measured densities of sintered and green samples, respectively. All possible values of p were tested and linear fit of the plot between $\ln\{T^{2/p}(\Delta l/l_o)\}$ and $1/T$ was evaluated. The best fit resulted with $p = 5$, i.e. for lattice/volume diffusion as the dominant process during initial stage of sintering. This is further supported by SEM micrographs recorded on samples sintered at 1023 K (Fig. 7) as discussed later. Fig. 2 shows the Arrhenius plots drawn using Eq. (1) with $p = 5$ for metal powders prepared at different temperatures and sintered in different atmospheres. The values of apparent activation energy 'Q_a', evaluated from the slopes of the linear fits were used to calculate the actual activation energy 'Q' using Eq. (3). The values are presented in Table 1. It is evident that the lowest activation energy is required for powder prepared at 823 K and sintered in Ar–4% H_2 atmosphere whereas sample sintered in pure argon atmosphere required maximum energy of activation.

The role of reducing atmosphere in lowering the activation energy as compared to inert atmosphere (pure argon) can be explained in a twofold manner. First is the chemical ability of hydrogen to react with surface layer of carbonates/oxides formed during passivation and convert it to metal again. This in turn minimizes the diffusion barrier present due to these surface layers. Also, hydrogen molecules diffuse into the pores interstitially and therefore facilitates the densification process via reaction with surface layers [13]. The second factor is the physical capability of hydrogen to act as a lattice defect catalyst [14] that facilitates the movement of point defects and dislocations during sintering and therefore lowers the activation energy.

Table 1
Activation energy 'Q' of sintering for cobalt green compacts for powders prepared at different temperatures and sintered in different atmospheres.

Decomposition temperature (K)	Sintering atmosphere	Activation energy (kJ/mol)
823	Ar–4% hydrogen	223
873	Ar–4% hydrogen	245
823	Pure argon	365

Suitability of powders decomposed at 823 K for attaining lowest activation energy of sintering can be explained as follows: regarding the powder properties, two opposing factors are operative simultaneously (i) particle size and (ii) surface layer on these particles. Smaller the particle size, faster is the diffusion resulting into low activation energy. On the other hand, larger surface area available with these smaller particles will lead to more surface layers (carbonates/oxides) acting a diffusion barrier and therefore slow down sintering. Powder obtained at 723 K with a smaller average particle size of 12 μm possesses higher surface contamination and therefore yields lower sintered densities with higher activation energies. On the other hand, powder decomposed at 873 K is coarse in nature with a larger particle size and lesser surface contamination, again leading to poor sintering kinetics. Therefore powder processed at 823 K has an optimum compromise between particle size and surface contamination and lead to faster sintering with lowest activation energy. The above reasoning is supported by results shown in the inset of Fig. 2 where maximum sintered density is achieved with powders processed at 823 K and compacted with a pressure of 250 MPa.

The above results of conventional sintering studies clearly establish the influence of powder processing conditions, sintering atmosphere and compaction pressure over the sintering kinetics and energy of activation. The results helped us in defining the optimum powder parameters for further dilatometric studies to investigate sintering mechanism.

3.3. Sintering studies by dilatometry: evidence of early shrinkage

Fig. 3 shows the shrinkage profiles of cobalt metal powder compacts sintered at different temperatures in thermo mechanical analyzer. It can be seen that maximum shrinkage is achieved for sample heated up to 1573 K yielding nearly 98% theoretical density

cobalt pellets. However, an interesting observation, as shown in the inset of Fig. 3 was noted in shrinkage profiles recorded in the earlier stages of heating. Instead of initial expansion, normally expected due to usual thermal expansion of any material before actual sintering commences, small amount of shrinkage was observed when sintered in reducing atmosphere (curve-a). On the other hand, sample sintered in pure argon atmosphere neither showed expansion nor contraction up to 823 K (curve-b). To check for the initial shrinkage observed below 823 K in the reducing atmosphere, a green pellet preheated up to 823 K in Ar–4% H_2 atmosphere for 1 h was subjected to dilatometer. The preheated compact yielded a normal shrinkage curve with expansion up to 900 K followed by actual sintering (curve-c). Also, it can be seen from the inset that actual sintering starts at quite low temperature at 830 K as compared to preheated compact that showed sintering only above 900 K. The initial shrinkage observed at temperatures below 823 K before the actual sintering can be explained as due to (i) reduction of surface contamination (carbonates/oxides) layers to metal and thus reducing the volume [6] and (ii) very high surface energy of the submicron sized powders that facilitate their aggregation at relatively lower temperatures and hence exhibit shrinkage.

3.4. Sintering kinetics using stepwise isothermal dialatometry (SID)

SID shrinkage data obtained from cobalt powder compacts have been analyzed by the method proposed by Makipirtti and Meng [8–11]. Before detailing the results, a brief description of this model is presented.

(i) Makipirtti–Meng method: according to Makipirtti–Meng equation for an isotropic sintering behavior, the fractional densification function, Y is expressed as

$$Y = \frac{V_o - V_t}{V_o - V_f} = \frac{{L_o}^3 - {L_t}^3}{{L_o}^3 - {L_f}^3} \quad (4)$$

where V_o (L_o), V_t (L_t), and V_f (L_f) are the initial volume (length), volume (length) at time t, and volume (length) of the fully-dense specimen, respectively. A normalized rate equation as suggested by Makipirtti–Meng method can be written as

$$\frac{dY}{dt} = nk(T)Y(1-Y)\left(\frac{1-Y}{Y}\right)^{1/n} \quad (5)$$

$$k(T) = k_o \exp\left(\frac{-Q}{RT}\right) \quad (6)$$

Here $k(T)$ is specific rate constant, k_o, the frequency factor, Q, the energy of activation, R, the gas constant and n, a parameter related to the sintering mechanism.

Fig. 4 shows the shrinkage profile and shrinkage rate of the green compact that was subjected to SID sintering schedule. It is clear from the curve that maximum shrinkage during a single isothermal soak period occurs at 1050 K with the maximum rate of shrinkage. The nature of shrinkage rate curve also indicates a probable change in the dominant mechanism of sintering during this isothermal period. The shrinkage data, after fitting into Eq. (5) are plotted

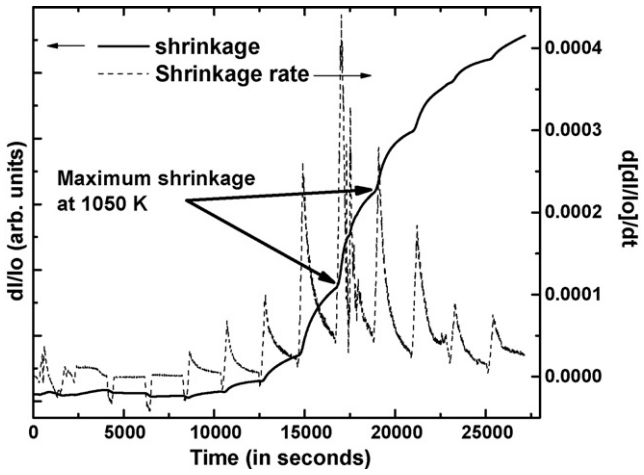

Fig. 4. SID shrinkage profile of cobalt green compact along with the shrinkage rate as a function of time.

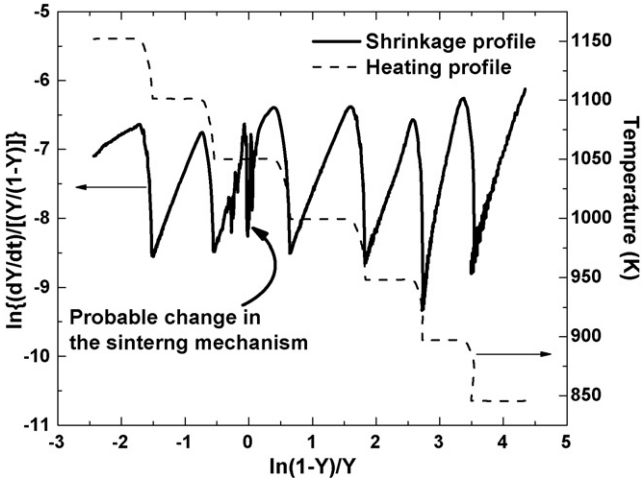

Fig. 5. Plots of $\ln\{(dY/dt)/[Y/(1-Y)]\}$ versus $\ln[(1-Y)/Y]$ according to Makipirtti–Meng equation. Variation of temperature is also shown on the right hand scale.

in Fig. 5 as $\ln(dY/dt)/[Y/(1-Y)]$ versus $\ln[(1-Y)/Y]$. A near straight line behavior for each isothermal hold zone except for 1050 K indicates that the model agrees well with the present sintering data of cobalt. A discontinuity in linearity for isothermal hold zone of 1050 K, indicated by an arrow further supports a probable change in the dominant mechanism of sintering during this period as was indicated by the shrinkage rate behavior in Fig. 4. The values of slope 'n' and intercept '$\ln k(T)$', evaluated by least-squares linear fitting for each straight line segment of the curve, are presented in Table 2. For the isothermal hold zone at 1050 K however, the slope calculated was from the linear fitting of the curve before the start of the discontinuity. Slope could not be calculated after the

Table 2
Kinetic analysis of SID shrinkage data of cobalt green compacts according to Makipirtti–Meng equation.

Temperature (K)	$1000/T$ (K^{-1})	$1/n$	n	$\ln(n)$	$\ln K(T)$	Regression parameter
790	0.00126	4.62	0.216	−1.5304	−18.47	0.9921
845	0.00118	4.54	0.220	−1.5138	−17.67	0.9937
900	0.00111	3.17	0.315	−1.1537	−15.06	0.9876
950	0.00105	3.13	0.319	−1.1410	−13.66	0.9924
1000	0.00100	2.81	0.355	−1.0338	−11.44	0.9906
1050	0.00095	2.66	0.375	−0.9788	−9.31	0.9942
1100	0.00091	2.77	0.361	−1.0188	−7.12	0.9925
1150	0.00087	2.71	0.369	−0.9969	−3.97	0.9941

completion of discontinuity at the same temperature due to the scattered nature of the data. Interestingly, parameter '*n*', that relates to the sintering mechanism takes nearly three different average values in the measured temperature range as $n \sim 0.218$ (790–850 K), 0.317 (900–950 K) and 0.365 (1000–1150 K). These values suggest that there are three different sintering mechanisms, operative as dominant processes over the above temperature intervals.

Fig. 6 shows the Arrhenius plot between $\ln k(T)$ and $1/T$ for SID shrinkage data. The curve can be fitted into three linear segments in the temperature ranges 790–850, 850–950 and 950–1150 K. The apparent activation energy '*Q*' was calculated from the slopes of each segment and compared with that of various sintering mechanisms reported in the literature [5,7]. The values are presented in Table 3. It is evident that sintering of cobalt powder compacts can be divided into three main stages. The first stage (790–850 K) relates to sintering within the aggregates which are formed upon coalescence of the individual crystallites and thereby leading to neck formation through grain boundary diffusion. This is further supported by the SEM image recorded on 850 K sintered sample that shows initial stage of neck formation (Fig. 7a). The higher value of activation energy (234 kJ/mol) for temperature range 850–950 K is an indicative of lattice (volume) diffusion as the dominant pro-

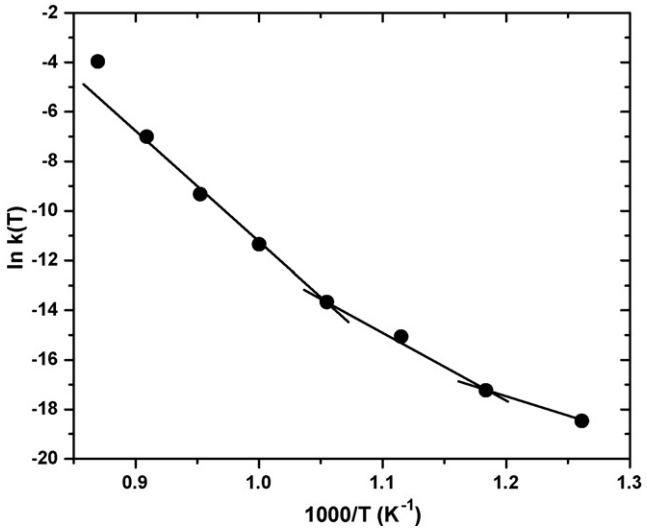

Fig. 6. Arrhenius plot of $\ln k(T)$ versus $1000/T$ based on the data in Table 3.

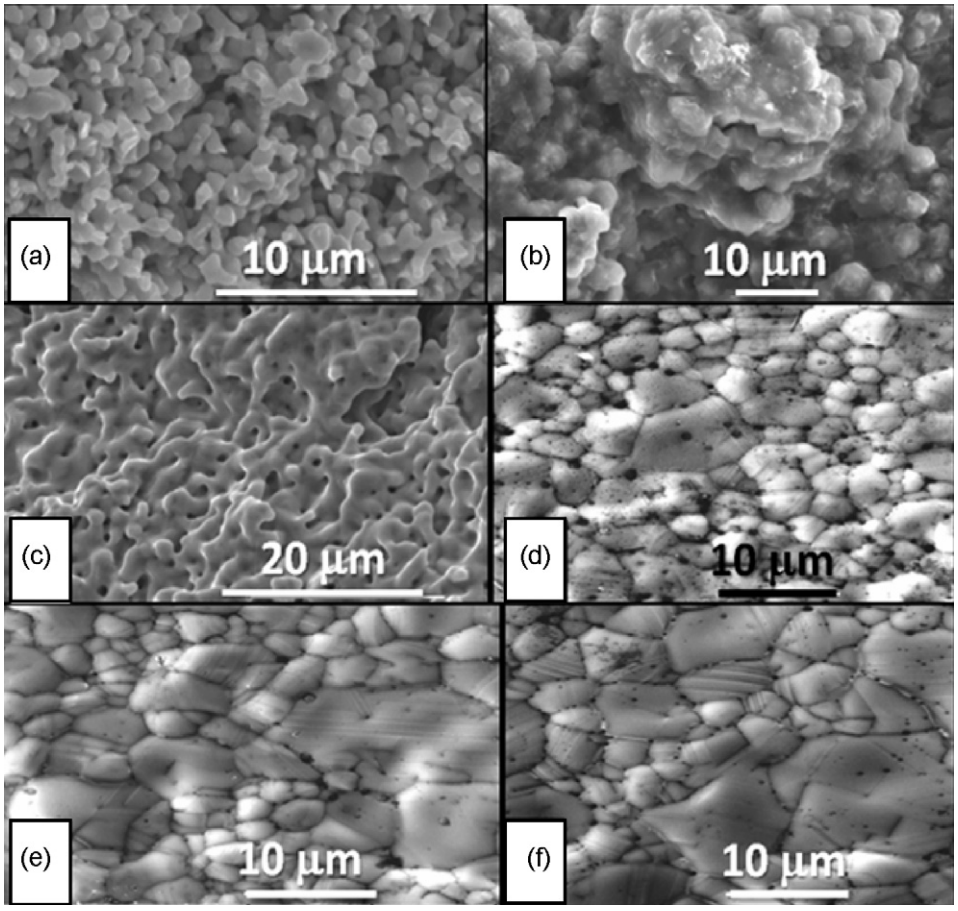

Fig. 7. SEM micrographs of fractured surfaces of cobalt samples sintered up to different temperatures: (a) 850 K, (b) 950 K, (c) 1100 K, (d) 1273 K, (e) 1373 K, and (f) 1473 K.

Table 3
Values of activation energies along with the literature values and corresponding sintering mechanism as evaluated from the Arrhenius plot obtained from Makipirtti–Meng's method.

Temperature range (K)	Activation energy (kJ/mol)	Mechanism of sintering	Literature value (kJ/mol)
790–850	135	Grain boundary	163 [5]
850–950	234	Lattice/volume diffusion	289 [5]
950–1150	373	Viscous/plastic flow	261–304 [7]

cess for mass transport. The same is supported by SEM micrograph recorded on a sample sintered up to 950 K as shown in Fig. 7b. The relatively lower values of activation energies for these two stages as compared to literature reported values is due to fine sized particles rendering larger interfaces, more defects, etc. [15]. In the third stage (950–1150 K), sintering mainly occurs by viscous flow/plastic flow along with other mechanisms also taking part and therefore required maximum energy of activation. The viscous/plastic flow of cobalt can be seen from the SEM images recorded on 1100 K sintered sample (Fig. 7c). Actually, due to the low stacking fault energy of cobalt, it has a tendency to show dynamic recrystallization in the temperature range from 900–1200 K [16]. A large number of dislocations that were generated during the cold compaction of cobalt powder get annihilated in this stage of plastic flow and result into recrystallized form of the parent structure. The micrograph recorded on sample sintered at 1273 K (Fig. 7d) clearly reveals the same. Successive grain growth with increasing temperature can be seen in Fig. 7e and f recorded on samples sintered at 1373 and 1473 K, respectively.

From the above discussion, it is therefore quite clear that the SID approach can well be used to evaluate the sintering kinetics of metallic systems and can give fairly reliable values of the activation energies involved with different mechanism of mass transport using the dilatometry data of a single experiment. The results are found to be consistent with the microstructural evaluation as studied by SEM analysis.

4. Conclusion

Sintering kinetics of submicron sized fine cobalt metal powder prepared through oxalate decomposition route was studied by both conventional sintering technique and stepwise isothermal dilatometry (SID) technique. Experimental results demonstrate that factors like powder preparation temperature, compaction pressure and sintering atmosphere play an important role in attaining optimum sintered density and fast sintering with lowest activation energy. Small amount of shrinkage observed at low temperatures before the start of actual sintering was due to fine sized nature of powder and reduction of surface carbonate/oxide layers in reducing atmosphere. SID shrinkage data were analyzed by Makipirtti–Meng method to evaluate the sintering mechanism and activation energies. The method was found to fit well with the shrinkage data of cobalt and hence validated its applicability for sintering studies of metallic powders also. Sintering was found to occur through three dominant mechanisms with average activation energies of 135, 234 and 373 kJ/mol corresponding to grain boundary diffusion, lattice diffusion and plastic/viscous flow, respectively. The results were found to be consistent with the microstructural evaluation as studied by SEM analysis.

Acknowledgements

The authors wish to acknowledge Dr. A.K. Suri, Director, Materials Group, BARC and Dr. D. Das, Head, Chemistry Division, BARC for their constant encouragement and support during the course of this work.

References

[1] I.G. Sharma, Studies on preparation and characterization of cobalt powder and its fabrication into cobalt rods, Ph.D. Thesis, Mumbai University, India, 2006.
[2] J.A. Ylikerala, M. Gasik, Powder Report 59 (2004) 36.
[3] M.V. Rane, V.H. Bafna, R. Sadanandam, A.K. Sharma, K. Ramadevi, N.K. Menon, M.F. Fonseca, S.K. Tangri, A.K. Suri, Hydrometallurgy 77 (2005) 247.
[4] R. Sadanandam, M.F. Fonseca, K. Srikant, A.K. Sharma, S.K. Tangri, A.K. Suri, Hydrometallurgy 91 (2008) 28.
[5] J.P. Jernot, J.L. Chermat, A. Deschanvres, B.L. Mordike, Materials Research Bulletin 17 (1982) 815.
[6] Y. Sakka, Journal of Less Common Metals 168 (1991) 277.
[7] K. Saitou, Scripta Materiallia 54 (2006) 875.
[8] R. Yan, F. Chu, Q. Ma, X. Liu, G. Meng, Materials Letters 60 (2006) 3605.
[9] G.Y. Meng, O.T. Sorensen, in: T. Han (Ed.), Advanced Structural Materials, vol. 2, Elsevier Science Publishers B.V., Amsterdam, Netherlands, 1991, p. 369.
[10] H.T. Wang, X.Q. Liu, F.L. Chen, G.Y. Meng, Journal of American Ceramic Society 81 (1998) 781.
[11] Y.F. Liu, X.Q. Liu, S.W. Tao, G.Y. Meng, O.T. Sorensenb, Ceramic International 28 (2002) 479.
[12] R.M. German, Powder Metallurgy Science, 2nd ed., MPIF, Princeton (NJ), 1994, 250.
[13] L. Liu, N.H. Loh, S.B. Tor, Y. Murakoshi, R. Maeda, Scripta Materialia 55 (2006) 1103.
[14] O. Dominguez, J. Bigot, Nanostructured Materials 6 (1995) 877.
[15] V.V. Dabhade, T.R. Rama Mohan, P. Ramkrishnan, Materials Science and Engineering A 452 (2007) 386.
[16] B. Paul, R. Kapoor, J.K. Chakravartty, A.C. Bidaye, I.G. Sharma, A.K. Suri, Scripta Materialia 60 (2009) 104.